Large-scale flow organization of wall-bounded turbulence over flush-mounted rotating discs

Kempaiah, Kushal U.; Sem, Jacopo; Baars, Woutijn J.

12th International Symposium on Turbulence and Shear Flow Phenomena (TSFP12)
Osaka, Japan, July 19–22, 2022

LARGE-SCALE FLOW ORGANIZATION OF WALL-BOUNDED TURBULENCE OVER FLUSH-MOUNTED ROTATING DISCS

Kushal U. Kempaiah
Faculty of Aerospace Engineering
Delft University of Technology
2629 HS Delft, The Netherlands
k.ujjainikempaiah@tudelft.nl

Jacopo Sem
Faculty of Aerospace Engineering
Delft University of Technology
2629 HS Delft, The Netherlands

Woutijn J. Baars
Faculty of Aerospace Engineering
Delft University of Technology
2629 HS Delft, The Netherlands

ABSTRACT

Rotating discs, flush-mounted within the wall beneath a turbulent boundary layer, affect the large-scale flow dynamics. An organized array of rotating discs is a surrogate for the transverse-oscillating wall concept that is known to reduce turbulent friction drag, since the convecting flow encounters a travelling wave, particularly in the spanwise centre of the discs. This work experimentally assesses the flow manipulation of this wall-based actuation method using planar and stereoscopic particle image velocimetry (PIV). Experiments were conducted in a developing turbulent boundary layer, at $Re_\tau \approx 910$, and with an optimized viscous-scaled sizing and layout of the discs following the direct numerical simulation (DNS) study of Ricco & Hahn (2013). Planar PIV in the streamwise–wall-normal plane over the spanwise centre of the discs revealed a reduction of the in-plane Reynolds stresses, suggesting a suppression of the near-wall turbulence auto-generation process. Wall-parallel planes of velocity data at a height of 70 viscous units above the wall revealed two distinct types of streamwise-oriented regions, comprising low- and high-momentum pathways. These spanwise alternating regions were also captured using the stereo-PIV measurements downstream of the disc-array. It was observed that the mean boundary layer flow is pulled closer to the wall in the disc center, resulting in a higher mean velocity and a less intense streamwise Reynolds stress for a given wall-normal height. With this effect being maximum in the disc center, while being absent between the discs, this type of flow manipulation could be optimized in terms of turbulence suppression (and potentially in terms of friction drag reduction at high Reynolds numbers), by considering larger discs.

INTRODUCTION

An active flow control method for turbulent friction drag reduction, relying on transverse wall-oscillation at time-scales matching the most energetic temporal scales of the near-wall turbulence ($t^+ \approx 100$) has been studied extensively for over 30 years (Leschziner, 2020). In a DNS study of Quadrio & Ricco (2004), a reduction in friction drag of up to 45% was reported, albeit this study was limited to a friction Reynolds number of $Re_\tau = 200$ (note that $Re_\tau \equiv \delta u_\tau/\nu$ or δ^+ is the ratio of the channel half-width or boundary layer thickness δ, to the viscous length scale ν/u_τ). Recently, Kempaiah *et al.* (2020) conducted experiments on a transverse oscillating wall and explored an oscillating time-scale down to $t^+ = 94$ at a Reynolds number of $Re_\tau = 570$; their results were in line with the earlier DNS studies of Quadrio & Ricco (2004) in terms of friction drag being higher when approaching the temporal scale of near-wall turbulence. Since the working mechanism of this global actuation method relies on a motion that scales with the viscous time-scale, an experimental implementation of this actuation method is practically challenging when moving towards higher Reynolds numbers, primarily due to high inertial and vibrational forces required to sustain the high-frequency oscillation.

Recently, Marusic *et al.* (2021) postulated that a more effective drag reduction at high Reynolds number conditions can be achieved with wall-oscillation frequencies on the order of large, outer-scaled flow features. Still, the current work focuses on relatively low Reynolds number conditions and follows the control concept of Keefe (1997). He proposed a wall-normal vorticity-forcing through an array of flush-mounted discs within the wall, each rotating at a constant angular velocity (top view in fig. 1c). That is, each disc belonging to a spanwise row in a streamwise–spanwise array, rotates with the same orientation, but alternates from row-to-row. In this way the convective flow encounters a degree of spanwise wall-oscillation. The wave motion is perpendicular to the flow and maximum in amplitude when considering the spanwise centre of a streamwise line of discs. Note that a practical implementation of this actuation method is relatively easy: it does not require any oscillatory, linear motion, but is only based on rotational motion. This control concept was examined using DNS of channel flow by Ricco & Hahn (2013), who

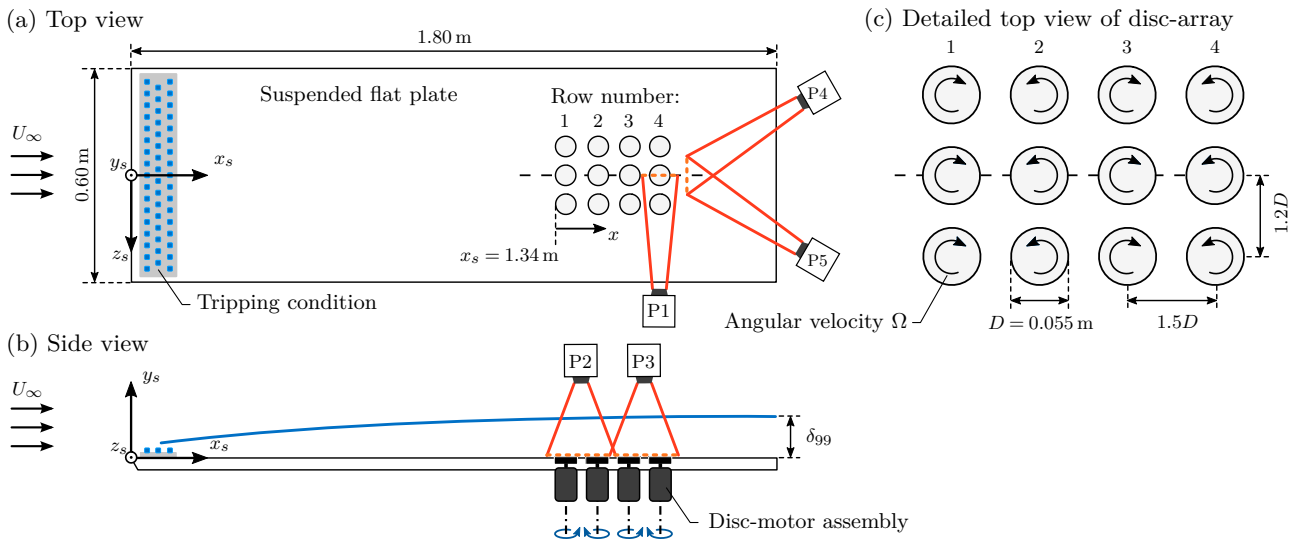

Figure 1: Schematic of the experimental TBL flow setup, with the array of rotating discs flush-mounted in a flat plate. Acquisition planes of PIV measurements and camera placements are also indicated (not to scale).

inferred maps of friction drag reduction as a function of the viscous-scaled disc diameter ($D^+ \equiv Du_\tau/\nu$) and edge velocity ($W^+ \equiv W/u_\tau$ with $W = 0.5D\Omega$, in which Ω is the angular rate-of-rotation); a maximum wall-drag reduction of 23% was found at a friction Reynolds number of $Re_\tau = 180$.

Our current work explores the wall-based actuation method of turbulent boundary layer (TBL) flow at Reynolds numbers higher than the ones available in the literature, and using an experimental implementation of the technique (Sem, 2021). To the authors' knowledge, this is the first practical realization of this type of flow control method and a description of the hardware, as well as the PIV-based velocity measurements for assessment of the large-scale flow organization, are covered next.

EXPERIMENTAL CAMPAIGN

Wind tunnel and array of rotating discs

Experiments were conducted in an open-return low-speed wind tunnel at the Faculty of Aerospace Engineering of the Delft University of Technology. A boundary layer with a slight favorable pressure gradient was generated using a flat plate comprising a width of 0.60 m and a length of 1.80 m (fig. 1a). The boundary layer was tripped using distributed roughness elements of 1.0 cm in height, following the work of Kempaiah *et al.* (2020). Throughout this paper, coordinates x, y and z denote the streamwise, wall-normal and spanwise directions of the flow, and lower-case u, v and w represent the Reynolds decomposed fluctuations of velocity, respectively. TBL parameters are listed in table 1 and were determined from the measured velocity profile of the uncontrolled flow (fig. 2a, described later).

An array of 4×3 flush-mounted rotating discs was designed per the optimal case in terms of the largest drag reduction identified by Ricco & Hahn (2013): a disc diameter of $D^+ = 550$ and a disc-edge velocity of $W^+ = 10$. Even though their Reynolds number was relatively low ($Re_\tau = 180$), this type of actuation method

Table 1: TBL parameters at $x_s = 1.535$ m.

Re_τ	Re_θ	δ	θ	u_τ	H
910	1950	87 mm	8.8 mm	0.15 m/s	2.03

targets the near-wall cycle turbulence and should therefore adhere to a viscous scaling. With the current boundary layer parameters of table 1, the disc diameter became $D = 0.055$ m. The array was constructed with streamwise and spanwise spacings of 0.083 m ($1.5D$) and 0.065 m ($1.2D$), respectively, to allow mounting of the DC electric motors to the bottom side of the plate. Each motor contained a double ball-bearing shaft to which the discs were directly mounted. All motors were powered with a single power supply and their angular velocities, Ω, were measured using a tachometer. Variations in Ω of each individual disc were less than 3% of the mean Ω. This work includes results corresponding to two different edge velocities, $W^+ = 10$ and $W^+ = 25$. So the former corresponds to the largest friction drag reduction, while the latter should result in an increase of friction drag (see fig. 4b of Ricco & Hahn, 2013).

Particle image velocimetry

Planar-PIV measurements were performed in two configurations, being (1) a streamwise–wall-normal (x, y)–plane, and (2) a wall-parallel (x, z)–plane. The (x, y)–plane measurements were conducted over the centreline of the most downstream disc, and were imaged using a single camera, labelled as 'P1' in fig. 1a. The (x, z)–plane measurements were performed using two cameras ('P2' and 'P3' in fig. 1b) and the total field-of-view (FOV) covered the entire disc-array. The exact height of the wall-parallel plane ($y^+ = 70$) was determined a-posteriori by comparing the mean velocity in the plane to the mean velocity profile extracted from the (x, y)–plane measurements. Finally, stereo-PIV measurements were performed in a wall-normal–spanwise (y, z)–plane, downstream of the aft-centre disc

Table 2: Summary of PIV measurements (note: different configurations were not acquired simultaneously).

Config.	Type	Plane	# of cameras	Field-of-view	Image res.	Interog. window	Vector pitch
1	Planar	(x,y)	1 (P1)	$75\times63\,\mathrm{mm}^2$	$34\,\mathrm{px/mm}$	$32\times8\,\mathrm{px}^2$	$0.12\,\mathrm{mm}$
2	Planar	(x,z)	2 (P2 & P3)	$250\times210\,\mathrm{mm}^2$	$10\,\mathrm{px/mm}$	$24\times24\,\mathrm{px}^2$	$0.25\,\mathrm{mm}$
3	Stereo	(y,z)	2 (P4 & P5)	$55\times55\,\mathrm{mm}^2$	$30\,\mathrm{px/mm}$	$64\times64\,\mathrm{px}^2$	$0.50\,\mathrm{mm}$

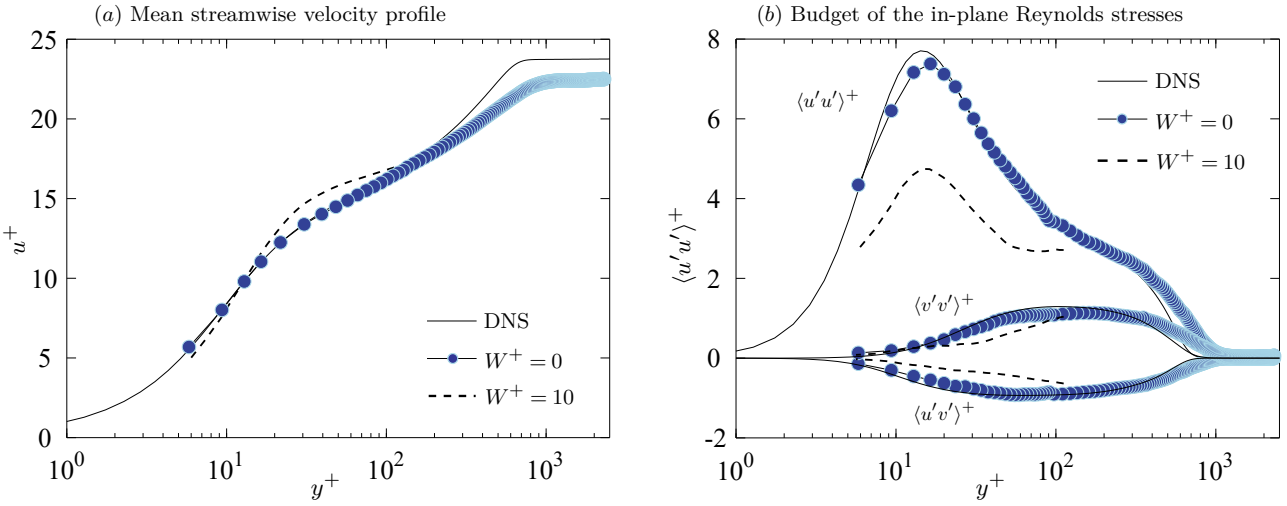

Figure 2: (a) Streamwise mean velocity profile for the uncontrolled ($W^+=0$) and controlled ($W^+=10$) cases, and (b) the corresponding profiles of all Reynolds stresses in the (x,y)–plane. Only every 2nd PIV data point is shown for clarity of the graphs, and DNS profiles are taken from Schlatter & Örlü (2010).

at $x_s = 1.67\,\mathrm{m}$ (roughly $0.45D$ behind the disc-array). Two cameras were employed ('P4' and 'P5' in fig. 1a) and were situated outside of the flow, placed at a stereoscopic angle of 55°.

For PIV acquisition, the flow was seeded with fog droplets of $1\,\mu$m diameter, produced with a SAFEX fog generator. Illumination was provided by a Quantel Evergreen 200 laser (Nd:YAG, $2\times200\,\mathrm{mJ}$, $15\,\mathrm{Hz}$) and the laser sheet thickness was on the order of 1 mm. Images were captured using LaVision Imager sCMOS cameras ($2560\times2160\,\mathrm{px}^2$, 16 bits and $6.5\,\mu$m pixel size) equipped with Nikon lenses of 105 mm focal length. Post-processing employed an image interrogation using the multi-pass cross-correlation (including window refinement and deformation, Scarano & Riethmuller, 2000); non-isotropic windows were used for the (x,y)–plane measurements to increase the wall-normal resolution. Further details of the PIV processing and resolutions of the velocity fields are provided in table 2.

BOUNDARY LAYER PROFILES

Figures 2a and 2b present profiles of the mean velocity and the Reynolds stresses, respectively. Profiles are generated by streamwise averaging the (x,z)–plane PIV data over the streamwise extent of the aft disc. First, the profiles of the uncontrolled case ($W^+=0$) are compared to profiles of DNS data of TBL flows, extracted from Schlatter & Örlü (2010). The wall-normal trends from the experimental data, of both the mean velocity u and the Reynolds stresses $\langle u_i'u_j'\rangle^+$, show a good agreement with the DNS data in the inner region. Discrepancies in the outer-region are described to the favorable pressure gradient of the experimental flow (constant cross-sectional area wind tunnel in which the flat plate is suspended).

For the case of optimal control ($W^+=10$), velocity data is available only for $y^+<100$. That is, the FOV was decreased in size to achieve a higher near-wall resolution. When inspecting the mean velocity profile (scaled by the u_τ of the uncontrolled case), it is evident that the velocity decreases below $y^+\approx10$. This indicates a reduction of the average friction drag at the centre-spanwise location where the measurement was taken. Moreover, a peak-to-peak reduction of 30% in $\langle u'u'\rangle^+$ occurs, together with significant reductions in the magnitudes of $\langle u'v'\rangle^+$ and $\langle v'v'\rangle^+$ below $y^+\approx100$. A reduction of the mean velocity and turbulence intensities is associated with a reduction in turbulent friction drag generation (Baron & Quadrio, 1995). Note that our study is the first demonstration-experiment, but that a direct determination of the reduction in friction drag was not reliable, due to wall-reflections of the rotating discs and minor vibrations in the setup (requiring an adaptation of the structure). As a consequence of the non-uniform actuation in the span, the wall-drag modification also depends strongly on the z location (and x), as detailed in the work of Ricco & Hahn (2013). Nevertheless, we here continue with a description of how the rotating disc-array affects the large-scale flow organization. For this we inspect the other two PIV measurement configurations, described next.

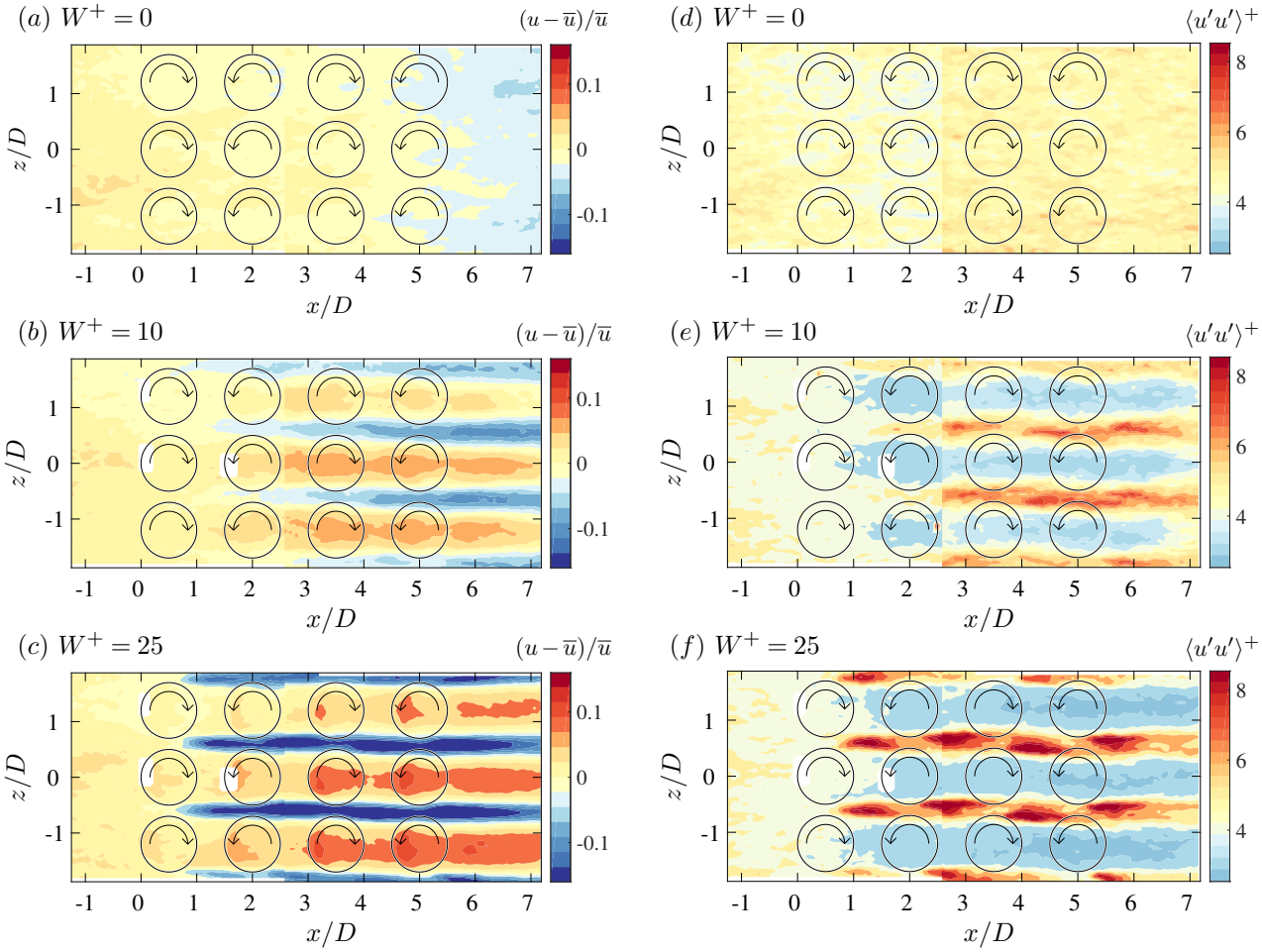

Figure 3: (a-c) Contours of the in-plane streamwise velocity, where $\overline{u}$ is the mean velocity of the entire wall-parallel plane of the uncontrolled case, $W^+ = 0$. (d-f) Contours of the streamwise Reynolds stress, all normalized with the u_τ in table 1. Edges of the discs, and their rotation direction, are drawn in black; small white regions mask spurious vectors, which were a consequence of laser reflections on the discs.

LARGE-SCALE FLOW ORGANIZATION

Wall-parallel plane

The normalised streamwise velocity in the wall-parallel plane at a height of $y^+ = 70$ (fig. 3a-c) shows low- and high-momentum pathways, in streamwise-aligned regions over the centre of the discs and in between them, respectively. For the case of optimal control ($W^+ = 10$), the flow over the spanwise-centred disc most aft in the array has a higher velocity, being consistent with fig. 2a. It is evident that the increase and decrease of the velocity in these low- and high-momentum pathways is strengthened when moving towards the case of $W^+ = 25$ (fig. 3c). For all cases, the mean velocity slightly decreases towards the end of the measurement region ($x/D \to 7$) because of the streamwise development of the TBL flow. The effect of control also increases significantly with downstream distance, due to the relatively short extent of the array in x.

Recall that a relatively high-speed region at $y^+ = 70$ corresponds to a relatively low-speed region lower in the boundary layer. In this context, the occurrence of low-momentum pathways very close to the wall, over the spanwise centre of the discs, was attributed to a viscous sub-layer being produced by a radial flow from the von Kármán pumping effect that is highly pronounced in the regions between the discs (Wise *et al.*, 2014). Wall-parallel planes of velocity at lower heights are challenging to acquire, due to laser wall-reflections and alignment issues and the current planes are therefore a surrogate of the trends very near-the wall, when interchanging the low- and high-momentum pathways. In order to make a qualitative comparison of how the mean flow is organized in the spanwise direction, the wall-parallel planes are streamwise-averaged in the region downstream of the aft row of discs, in the range $5.5 \leq x/D \leq 7$. The spanwise profiles for all cases of W^+ are shown in fig. 4. Notably, the regions of a velocity deficit in the case of control is narrower than the region of velocity surplus, but is more intense. Averaging the spanwise velocity over one periodic-unit of the flow ($-0.6 \leq z/D \leq 0.6$) yields the three vertical lines in fig. 4, indicating a monotonic trend towards a higher mean velocity when W^+ increases. Only when the wall-normal profiles (varying along the span) collapse in outer-scaling (adhering to a so-called 'outer-layer similarity'), at this wall-normal height, the spanwise trend and thus the average can be a surrogate for the spanwise variation in friction drag, An interpretation of fig. 4 in this context is too speculative, given that the outer-layer similarity has not been confirmed, because of the relatively low acquisition location of the

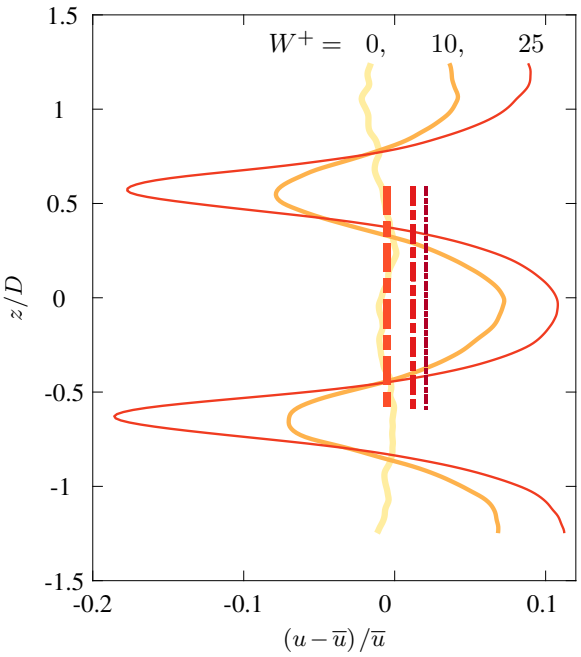

Figure 4: Spanwise profiles of the streamwise-averaged u-velocity component of figs. 3a-c, in the range $5.5 \leq x/D \leq 7$. Spanwise averages of these profiles, for one periodic-unit, are shown with the vertical lines for the range $-0.6 \leq z/D \leq 0.6$.

wall-parallel plane (below the onset of the logarithmic layer at $y^+ = 100$), and because of the streamwise development still taking place at the aft end of the array. Regardless, the current results show that the actuation method using rotating discs can establish low- and high-momentum pathways; the implications of this for future studies of this control technique are further discussed in the next section considering the cross-planes of velocity.

A final remark about the data in the wall-parallel plane is concerned with the regions of high and low Reynolds stress $\langle u'u' \rangle^+$, in comparison to the uncontrolled case. When focusing on the intense (red) patches of $\langle u'u' \rangle^+$ in figs. 3e,f, it is observed that these are located just downstream of each row of discs. When accepting that coherent turbulent structures are inclined by roughly 20° relatively to the wall, the observations at $y^+ = 70$ originated from the wall at a distance of $\Delta x^+ = 70/\tan(20°)$ upstream, equating to $\Delta x/D \approx 0.36$. This upstream shift would align the red patches of intense $\langle u'u' \rangle^+$ with the 'narrow passages' in between the discs. Their spanwise location depends on the rotation-direction of each row of discs.

Cross-plane downstream of array

Figure 5 displays data of the cross-plane stereo-PIV field, located just aft of the array. For both the uncontrolled ($W^+ = 0$) and optimal control case, the fields of the mean streamwise velocity u and Reynolds stress $\langle u'u' \rangle^+$ are shown. Note that the spanwise range covers the span of the disc located at $z = 0$. In comparison to the spanwise-invariant mean flow of the uncontrolled case, a clear spanwise modulation of the velocity isocontours appears in the case of $W^+ = 10$. This reflects the same observations that were made in fig. 4 (the wall-normal height of the wall-parallel plane is shown with the horizontal dashed line in all sub-plots of fig. 5): for a given height above the viscous sublayer, a higher mean velocity occurs in the disc centre, while the flow velocity is lower at the edges of the disc. Thus, the flow over the centre of the disc exhibits less momentum-deficit. From the topology of $\langle u'u' \rangle^+$ it is evident that for approximately $-0.25 \leq z/D \leq 0.25$, the streamwise Reynolds stress is constant in span and suppressed in comparison to the uncontrolled case.

At this stage it is worth mentioning that the large-scale flow organization over the disc array is strongly reminiscent of the one found over other wall-bounded turbulent flows with spanwise varying surface conditions. Specifically, wall-bounded turbulence convecting over walls with streamwise-aligned patches of (various degrees of) roughness, with a spanwise periodicity, are known to include large-scale secondary flows and the low- and high-momentum pathways discussed earlier with the aid of fig. 3. Details of such flows can be found elsewhere (Nugroho *et al.*, 2013; Barros & Christensen, 2014; Vanderwel & Ganapathisubramani, 2015, among others). A main difference between those flows and the one currently studied is that our actuation method achieves the spanwise varying friction drag with hydrodynamically-smooth rotating discs (having no pressure drag). To the contrary, the aforementioned studies in the literature comprise walls with pressure drag (e.g., streamwise-aligned roughness-patches of a certain width). The actuation method with the rotating disc does come however with a non-negligible power requirement for rotating the discs (Ricco & Hahn, 2013). All in all, having demonstrated that this actuation method is capable of establishing large-scale flow (re)organization, the variation in control 'authority' in terms of disc sizing, layout, and rate-of-rotation makes this actuation method an attractive candidate when exploring control of high Reynolds number flows. Those conditions remain unexplored with DNS and the current experimental work is a step towards this.

CONCLUDING REMARKS

An experimental investigation of the large-scale flow organization over an array of flush-mounted rotating discs under a turbulent boundary layer was conducted. Different configurations of PIV measurements were employed to reveal (and confirm in relation to the available literature on the topic) that low- and high-momentum pathways are established in the flow, due to the spanwise varying friction drag. It was recently found in a study with a fixed spanwise varying surface treatment that the spanwise wavelength (or disc size) governs the size and strength of the secondary flows (Wangsawijaya & Hutchins, 2022). In that study, the authors interpreted the secondary flows as spanwise-locked large-scale turbulent structures that are present even in smooth-wall turbulent boundary layers (but without preferred spanwise positioning). It is postulated that the actuation method using flush-mounted rotating discs will have a large control authority for the organization of large-scale flow features; this can be beneficial in terms of friction drag reduction technologies at high Reynolds number conditions. Particularly due to the total absence of pres-

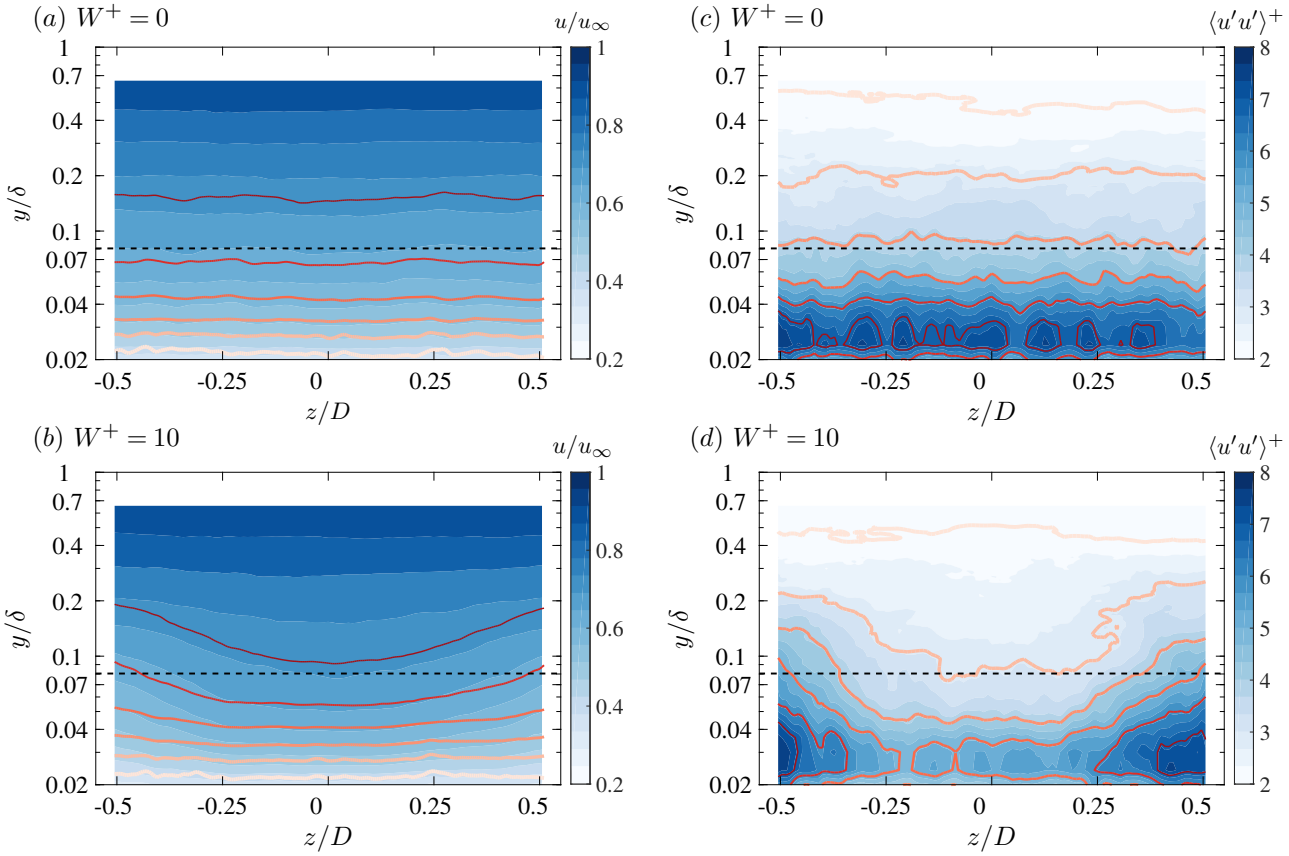

Figure 5: Contours of (a,b) the streamwise velocity and (c,d) the streamwise Reynolds stress for both $W^+ = 0$ and $W^+ = 10$. Note that the ordinate has a logarithmic scale. For clarity, the set of red-shaded lines on (a,b) are iso-contours at $u/u_\infty = 0.2 : 0.1 : 0.7$ and the lines on (c,d) are iso-contours at $\langle u'u' \rangle^+ = 2 : 1 : 7$.

sure drag with this control system (but, the power for spinning the discs should be accounted for). In the future, it will be interesting to examine if discs can be sized/laid out to increase the benefit of the reduced flow-induced friction in the centre area of the discs, so that it leads to a global friction drag reduction.

REFERENCES

Baron, A. & Quadrio, M. 1995 Turbulent drag reduction by spanwise wall oscillations. *Appl. Sci. Res.* **55** (4), 311–326.

Barros, J. M. & Christensen, K. T. 2014 Observations of turbulent secondary flows in a rough-wall boundary layer. *J. Fluid Mech.* **748**, R1.

Keefe, L. 1997 A normal vorticity actuator for near-wall modification of turbulent shear flows. AIAA, Paper 2009-0547.

Kempaiah, K.U., Scarano, F., Elsinga, G. E., van Oudheusden, B. W. & Bermel, L. 2020 3-dimensional particle image velocimetry based evaluation of turbulent skin-friction reduction by spanwise wall oscillation. *Phys. Fluids* **32**, 085111.

Leschziner, M. A. 2020 Friction-drag reduction by transverse wall motion – a review. *J. Mechanics.* **36** (5), 649–663.

Marusic, I., Chandran, D., Roughi, A., Fu, M. K., Wine, D., Holloway, B., Chung, D. & Smits, A. J. 2021 An energy-efficient pathway to turbulent drag reduction. *Nat. Commun* **12**, 5805.

Nugroho, B., Hutchins, N. & Monty, J. P. 2013 Large-scale spanwise periodicity in a turbulent boundary layer induced by highly ordered and directional surface roughness. *J. Fluid Mech.* **41**, 90–102.

Quadrio, M. & Ricco, P. 2004 Critical assessment of turbulent drag reduction through spanwise wall oscillations. *J. Fluid Mech.* **512**, 251–271.

Ricco, P. & Hahn, S. 2013 Turbulent drag reduction through rotating discs. *J. Fluid Mech.* **722**, 267–290.

Scarano, F. & Riethmuller, M. L. 2000 Advances in iterative multigrid PIV image processing. *Exp. Fluids* **29** (1), S051–S060.

Schlatter, P. & Örlü, R. 2010 Assessment of direct numerical simulation data of turbulent boundary layers. *J. Fluid Mech.* **659**, 116–126.

Sem, J. 2021 Rotating discs for turbulent drag reduction: an experimental study. Master's thesis, Delft University of Technology, Delft, The Netherlands.

Vanderwel, C. & Ganapathisubramani, B. 2015 Effects of spanwise spacing on large-scale secondary flows in rough-wall turbulent boundary layers. *J. Fluid Mech.* **774**, R2.

Wangsawijaya, D. D. & Hutchins, N. 2022 Investigation of unsteady secondary flows and large-scale turbulence in heterogeneous turbulent boundary layers. *J. Fluid Mech.* **934**, A40.

Wise, D.J., Alvarenga, C. & Ricco, P. 2014 Spinning out of control: Wall turbulence over rotating discs. *Phys. Fluids* **26** (12), 125107.